AUSTIN, L.G., MENACHO, J.M. and PEARCY, F. A general model for semi-autogenous and autogenous milling. APCOM 87. Proceedings of the Twentieth International Symposium on the Application of Computers and Mathematics in the Mineral Industries. Volume 2: *Metallurgy*. Johannesburg, SAIMM, 1987. pp. 107 – 126.

A General Model for Semi-autogenous and Autogenous Milling

L.G. AUSTIN, J.M. MENACHO and F. PEARCY

Pennsylvania State University, Philadelphia, Penn., USA

This paper was the subject of a cross-disciplinary presentation under the chairmanship of Dr A.M. Edwards

The paper summarizes the current state of development of simulation models for SAG and FAG mills, and gives the results of recent investigations of the physical processes occurring in autogenous grinding. The breakage process is treated as the sum of three regions of breakage actions: normal breakage caused by nipping of particles between media (steel balls or pebbles); abnormal breakage caused by media when the particle or lump is too big in relation to the media to be readily nipped; and self-breakage resulting from the chipping fracture and abrasion of the tumbling action of rock lumps. Each region of breakage action has associated specific rates of breakage and primary progeny fragment distributions.

A simplified form of the model was used to predict the performance of an 8 m diameter SAG mill with L/D = 0.5 grinding a copper ore, and predicted maximum capacity and minimum kWh/ton at about 6% ball load at 25% total filling. Two FAG mills of L/D = 2 were necessary to give the same capacity, and the simulations indicated a lower kWh/ton for these mills. For this ore, both systems were technically feasible.

Introduction

Although the use of simulation models for the design of ball mills has advanced significantly in recent years,[1] progress has been slow in applying the concepts of specific rates of breakage and primary breakage distributions in the construction of simulation models[2-4] for semi-autogenous (SAG) and fully-autogenous (FAG) mills. This is largely because the physical processes of breakage occurring in these mills are more complex than those in ball mills. Several recent papers by Austin and co-workers[5-9] have investigated certain aspects of this problem.

In this paper, we will first summarize the current state of development as we see it and then use an approximate simplified form of the models to compare the performance of a typical SAG mill design (L/D = 0.5) with that of a representative FAG mill with L/D = 2. It is assumed that the reader is familiar with the concepts and symbolism of construction of mill models.[1]

Mill models

The basic mass balance

It is assumed that this type of mill approximates to a fully mixed reactor where the grate acts like a size classifier to prevent large material leaving the mill. The simple concept of residence time distribution loses meaning in such a system

because the residence time is determined by the rates of breakage of feed material to less than the grate size, so it is a complex function of the feed size distribution and specific rates of breakage. However, it is still convenient to define a mean residence time by solid hold-up W divided by solid feed rate, $\tau=W/F$. The basic mass balance is simple to write:

$$Fp_i=Ff_i+(W\sum_{j=1}^{i-1} b_{i,j}S_jw_j)-WS_iw_i,\quad i=1,2,....n$$

or

$$p_i = f_i+\tau(\sum_{\substack{j=1\\ i>1}}^{i-1} b_{i,j}S_jw_j)-\tau S_iw_i \qquad [1]$$

where p_i is the fraction of mill product in size class i; f_i is fraction of feed in size class i; S_i is the specific rate of breakage of size i material; $b_{i,j}$ is the fraction of material broken from size class j which appears in size class i; w_i is the fraction of hold-up of size class i; and n is the total number of size intervals.

There is evidence that material less than the grate size undergoes classification as it passes through the grate (see later). Therefore, the system is treated as shown in Figure 1, with material rejected by the grate thrown back into the mill charge with an equivalent internal circulation ration of C'. Since F'=(1+C')F, the mass balance of the apparent mill feed is

$$(1+C')Ff_i' = Ff_i + F(1+C')w_ic_i$$

where the value of c_i is the fraction of size i material returned to the mill. The value of C' is defined by

$$C'=\sum_i F(1+C')w_ic_i/\sum_i F(1+C')w_i(1-c_i)$$

$$=\sum_i w_ic_i/\sum_i w_i(1-c_i)$$

or

$$1+C' = 1/\sum_i w_i(1-c_i) \qquad [2]$$

Applying Eq. [1] to this system using $w_i = p_i'$ gives

$$w_i = \frac{f_i+\tau\sum_{j=1}^{i-1} b_{i,j}S_jw_j}{\tau S_i+(1+C')(1-c_i)} \qquad i=1,2,..n \qquad [3]$$

The equation is readily converted to the close-circuit form.

The hold-up in the mill of sizes less

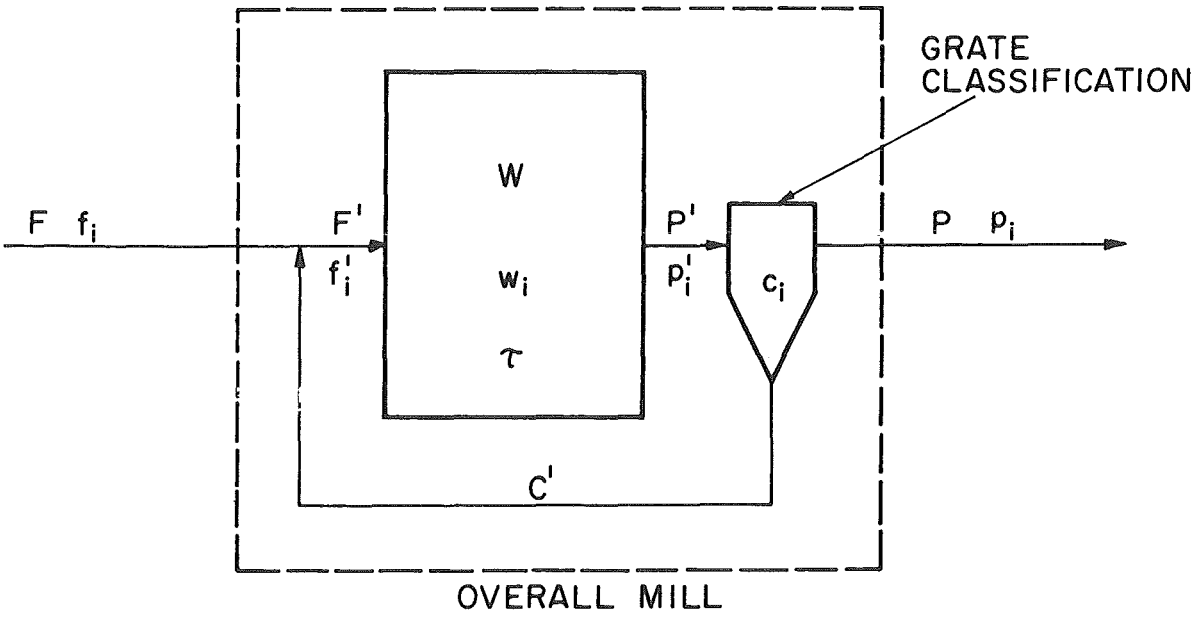

FIGURE 1. Illustration of grate classification treatment as an exit classifier

than the grate opening depends on the ease with which slurry flows from the mills: the level must increase in order to permit slurry to flow out at a higher rate. Thus, the system is only precisely defined if a mass transport relation is used. We will use the empirical function

$$f_s/f_{so} = (F_v/F_{vo})^{N_m} \quad [4]$$

where f_s is the fractional filling of the mill by slurry, with slurry defined by sizes less than the grate opening. F_v is a volume flow rate and N_m is an empirical constant. In terms of the hold-up of material of sizes less than grate opening in a mill of effective volume V,

$$f_s = \left(\frac{W}{\rho_s V C_s}\right) \sum_n^{i_g} w_k \quad [5]$$

where C_s is the volume fraction of solid in the slurry; ρ_s is the true density of the solid; and i_g is the interval number corresponding to the grate size. The value of F_{vo} is a standard flow rate which gives a standard filling of f_{so}. F_{vo} is expected[10] to be related to mill size by

$$F_{vo} = k_m \phi_c A_g D^{3.5} (L/D) \quad [6]$$

where ϕ_c is fraction of critical speed and A_g is the fraction of mill cross-section which is open grate area. The simultaneous solution of Eq. [4], [5] and [6] gives

$$\tau = \left(\frac{W}{F_{vo}\rho_s C_s}\right) \left(\frac{f_{so} C_s \rho_s V}{W \sum_n^{i_g} w_k}\right)^{1/N_m} \quad [7]$$

For given values of f_i, $b_{i,j}$, S_j and c_i there is only one value of τ which will satisfy both Eq. [3] and [7].

A more complex mass balance

The problem with the simple mass balance given above is that it considers overall first-order S_i values, whereas there is the possibility of a substantial component of abrasion in addition to normal breakage processes, and abrasion follows a different set of laws than breakage. Thus, Austin and Menacho[11] have formulated the overall balance on size i as 'Rate of size i material out= (rate of size i material in) + (net rate of material wearing in to size i by abrasion of rounded pebbles through the upper and lower limits of size interval i) - (rate of loss of fragments by abrasion of pebbles in size interval i) + (rate or production of size i material from the products of abrasion of larger sizes) - (rate of production of size i material by fracture) + (rate of production of size i material from the products of fracture breakage of larger sizes)'.

Considering abrasion according to a linear wear law it is readily shown[7,12] that the net rate of increase of mass due to pebbles of equivalent radius r wearing in and out of a differential size element dr is $W\kappa(d^2P/dr^2)dr$, where P is the cumulative mass fraction size distribution of hold-up W and κ is the linear wear rate (L/T). Similarly, the mass loss from the intervals is $(3\kappa/r)(dP/dr)dr$. Incorporating these with the usual first-order mass-rate balance due to fracture gives

$$Fp_i' = Ff_i' + W\int_{i+1}^{i} \frac{\kappa d(dP/dr)}{dr} dr - 3W \int_{i+1}^{i} \left(\frac{\kappa}{r}\right)\frac{dP}{dr} dr$$
$$+ 3W \sum_{j=1}^{i-1} a_{ij} \int_{j+1}^{j} \left(\frac{\kappa}{r}\right)\frac{dP}{dr} dr - S_i w_i W + W \sum_{j=1}^{i-1} b_{ij} S_j w_j$$

where a_{ij} is the fraction of material abraded from size j which appears in size interval i.

The value of κ is not necessarily constant over a wide size range but it can be assumed that it is approximately constant within a size interval; κ_i is thus defined as the mean value of κ for particle sizes $x_{i+1} < 2r < x_i$. Then

$$\int_{i+1}^{i} \kappa \frac{d(dP/dr)}{dr} dr = \kappa_{i-1} \frac{dP}{dr}\Big|_i - \kappa_i \frac{dP}{dr}\Big|_{i+1}$$

Also, by definition $\int_{i+1}^{i}(dP/dr)dr=w_i$, so it convenient to define a mean value $\bar{r}_i$ by the product of some factor σ and the upper size of sieve size i, $\bar{r}_i=\sigma x_i$ and make the reasonable approximation $\int_{i+1}^{i}(\kappa/r)(dP/dr)dr \cong \kappa_i w_i/\bar{r}_i$. The derivative dP/dr is approximated by $(dP/dr)_i \cong w_{i-1}/(x_{i-1}-x_i) \cong w_{i-1}/x_{i-1}(1-R)$, giving

$$p_i'=f_i'+\frac{\tau(\kappa_{i-1}w_{i-1}-\kappa_i w_i/R)}{x_1 R^{i-2}(1-R)}-\frac{3\kappa_i\tau w_i}{\sigma x_1 R^{i-1}}+\frac{3\tau}{\sigma x_1}\sum_{j=1}^{i-1}a_{ij}\kappa_j\left(\frac{w_j}{R^{j-1}}\right)-S_i w_i\tau+\tau\sum_{j=1}^{i-1}b_{ij}S_j w_j$$

where R is the ratio of lower to upper sieve size of the size interval ($=\sqrt{2}$).

It is convenient to define the specific rate of loss of material by abrasion to fragments as a fraction of the specific rate of fracture; letting $\gamma_i=(3\kappa_i/\sigma x_1 R^{i-1})/S_i$, putting $\sigma/3(1-R)=K$, and setting $p_i'=w_i$ gives as before

$$w_i=\frac{f_i+K\gamma_{i-1}\tau w_{i-1}S_{i-1}+\tau\sum_{j=1}^{i-1}(a_{ij}\gamma_j+b_{ij})S_j w_j}{(1+C')(1-c_i)+\tau\{S_i[1+\gamma_i(1+K)\ ]\ \}} \qquad [8]$$

to be used in place of Eq. [3] if abrasion processes are significant. The size distribution of the product stream from the grate classification is then given by $p_i=(w_i)(1+C')(1-c_i)$. For closed circuit the values of f_i are readily replaced in terms of make-up feed g_i using the s_i parameters for the external classifier.

FAG mill model

The FAG mill model is essentially identical to that to the SAG mill model given as Eq. [8] except that it is applied as an equivalent series of reactors[8,9] with various degrees of recycle of the material rejected back to the mill by the grate, as indicated in Figure 2. A grate classification action is necessary to retain the pebbles in the mill. Of course, the calculation of the effective overall S_i values will not include a term for breakage by balls. In addition, the mass transport constant k_m will correspond to that for a long L/D ball mill and not a short SAG mill.

Calculation of S and B values

Breakage by balls and pebbles

In order to allow for different ball and pebbles sizes in the mill, the values of specific rates of breakage of smaller sizes by impact from media were calculated from the equations developed for ball mills.[1] The relations between the specific rates of

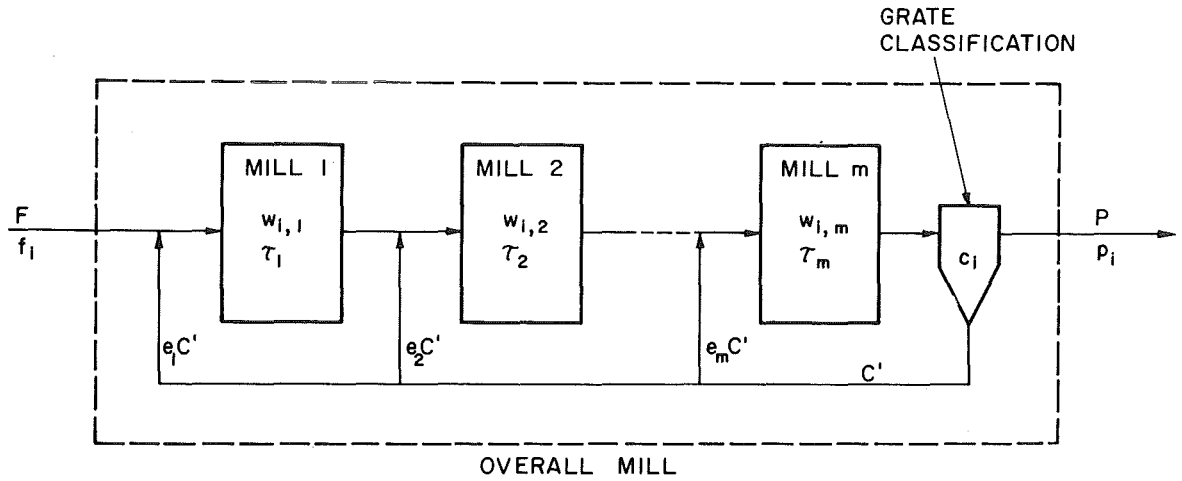

FIGURE 2. Reactors-in-series formulation for a FAG mill with grate classification

breakage determined using a single ball size in a laboratory test mill of diameter D_T and those for a mixture of balls in a larger mill of diameter D are

$$S_i=\Sigma m_k S_{i,k}= {}_T(\frac{x_i}{x_o})^{\alpha} (C_3)\Sigma_k \frac{m_k C_{2,k}}{1+(x_i/C_{i,k}\mu_T)^{\Lambda}}, \quad n>i\geq 1 \qquad [9]$$

$$S_n = 0$$

with

$$C_{1,k}=(D/D_T)^{N_2}(d_k/d_T)^{N_3} \qquad [10a]$$

$$C_{2,k}=(d_T/d_k)^{N_0} \qquad [10b]$$

$$C_3=(\frac{D}{D_T})^{N_1}(\frac{3.81}{D})^{\Delta}(\frac{1+6.6J_T^{2.3}}{1+6.6J^{2.3}})\exp[-c(U-U_T)]$$
$$(\frac{\phi_c-0.1}{\phi_{cT}-0.1})(\frac{1+\exp[15.7(\phi_{cT}-0.94)]}{1+\exp[15.7(\phi_c-0.94)]}) \qquad [10c]$$

where Δ=0 for SAG milling; Δ=0 for D<3.81 m and = 0.2 for D>3.81 m for ball milling or long L/D FAG milling.

The subscript T denotes conditions in the test mill, and m_k is the mass fraction of the k^{th} size class of balls in the full-scale mill: N_0, N_1, N_2, N_3 are empirical exponents based on experience with ball mills. The value of U is the fractional interstitial filling of the media voids by particles and J is the fractional filling of the mill by media. The values used for the exponents were N_1=0.5, N_2=0.2, N_3=1.0 and N_0=1.0, and the cushioning factor c was taken as 1.3.

The cumulative primary progeny fragment distributions ($B_{i,j}$) for normal breakage by a single size of ball of class k have been found to be fitted by the empirical function

$$B_{i,j,k}=\Phi_k(\frac{x_{i-1}}{x_j})^{\gamma_k}+(1+\Phi_k)(\frac{x_{i-1}}{x_j})^{\beta}, \quad i>j>1 \qquad [11]$$

as illustrated in Figure 3. For comparison purposes, the overall $B_{i,j}$ value for a mixture of balls can be calculated from

$$B_{i,j}= \Sigma_k m_k S_{j,k} B_{i,j,k} / \Sigma_k m_k S_{j,k} \qquad [12]$$

Figure 4 illustrates the decrease of breakage rates as the particles become too large to be nipped properly by the balls. In Region 2, the breakage of the material in a batch rate test becomes non-first order (abnormal) because it consists of a mixture of normal fracture caused by a direct impact and chipping caused by a glancing, less violent impact. Figure 3 shows the variation of overall B values as particle size increases with respect to the ball size. It is clear that chipping becomes more important as the size increases.

Equations [9] and [10] were used for both balls and pebbles, with the values of the characteristic parameters $_T$ and μ_T adjusted by

$$_T \text{ pebbles} = {}_T \text{ balls} \times \frac{\text{density pebbles } \rho_P}{\text{density balls } \rho_B} \qquad [13]$$

$$\mu_T \text{ pebbles} = \mu_T \times \rho_P/\rho_B \qquad [14]$$

The value of J to be used in Eq. [10c] is based on the total media filling which defines how media tumbles in the mill, that is, it must be the sum of filling by balls and pebbles, $J=J_B+J_P$. Calculation of breakage due to balls using this J would only be valid if all the media were steel, so the value is corrected by the factor of fractional volume J_B/J, $S(B)_i=(J_B/J)\ \Sigma\ m_k S(d_k)_i$. Similarly, $S(P)_i = (J_P/J)\ \Sigma\ w_j S(x_j)_i$ where w_j is the mass fraction of pebbles of size interval j in the tumbling charge. It is assumed that all rock larger than the grate size, plus balls, contributes to the media filling level of the mill.

The term $\exp[-c(U-U_T)]$ in Eq. [10c] represents the decrease of specific breakage rates when the media void spaces

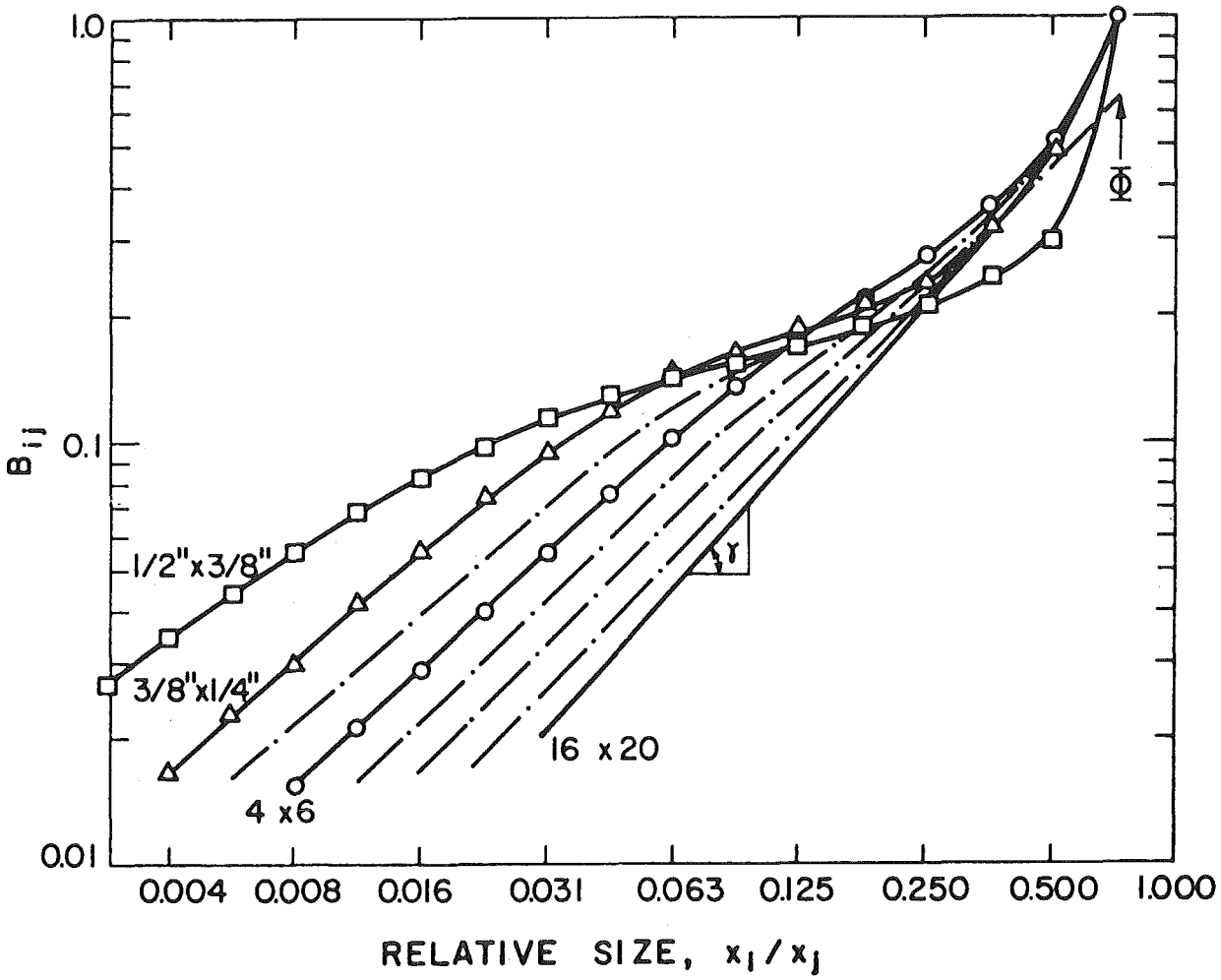

FIGURE 3. Typical variation of the breakage distribution values for large particles. Dry batch grinding of quartz in a 0.6 m diameter mill. U = 0.5, J_B = 0.2, 26.4 mm diameter balls, 75% of the critical speed

are overfilled. This effect states that excessive powder in the media cushions the breakage action on the powder. It seems reasonable that the cushioning action depends on the media size, that is, a 10 mm diameter lump will be media to small sizes but should be counted in the cushioning powder for pebbles of 100 mm diameter. Using the Weymont[13] voidage (η) factors a simple method of defining powder is that all material of size less than 0.125 of the media size is considered to be powder. This corresponds to a voidage factor of size i with respect to media size k of 0.5. Then the term in Eq. [10c] becomes $\exp[-c(U_k-U_T)]$, since the effective value of U depends on the media size being considered.

Self-breakage

As particle size is increased the particles are not nipped by tumbling balls. However, they eventually become big enough to break by the impact of their own fall, in the stream of tumbling rock and balls. Then the breakage rates increase with increased lump size due to the increased impact force, giving Region 3 of Figure 4. The transition from Region 2 to Region 3 is obtained by simple addition, $S_i=S(B)_i+S(P)_i+S(S)_i$ where $S(B)_i$ and $S(P)_i$ are breakage due to nipping by balls and pebbles (which become small at large sizes), and $S(S)_i$ has been termed self-breakage. The values of $S(S)_i$ appear also to follow a power function

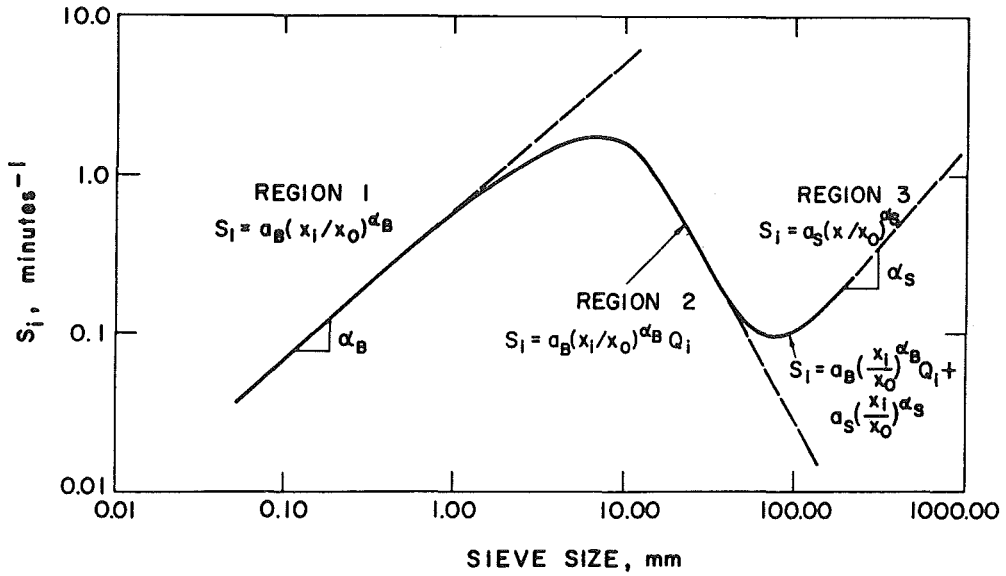

FIGURE 4. Typical shape for the sum specific rate of breakage in SAG

$$S(S)_i = {}_S(x_i/x_o)^{\alpha_S} \qquad [15]$$

where ${}_S$ is smaller than the corresponding for media, so that $S(S)_i$ is negligible for small particle sizes.

The empirical equation used to allow for the effect of media filling on self-breakage is

$$S(S)_i \propto \frac{1}{1+(J/0.4)^2} \qquad [16]$$

Since breakage is proportional to SJ, this gives a maximum rate of breakage at J=0.4. When a fraction of the media is steel balls it seems logical that the rock in the tumbling stream will receive a proportionate fraction of heavier impacts. Therefore, the breakage rates were corrected by

$$S(S)_i = (J_B\rho_B + J_P\rho_P)/J_P\rho_P \qquad [17]$$

Thus, although the breakage rate of a given size of tumbling rock is termed self-breakage it is accepted that the size and density of the rest of the charge has an influence on this breakage.

It is expected that the specific rates of self-breakage will scale with mill diameter in essentially the same way as breakage by balls as in Eq. [10]. Combining equations gives

$$S(S)_i = {}_{ST}(x_i/x_o)^{\alpha_S} C_{S1} C_{S2} \qquad [18]$$

where

$$C_{S1} = \begin{cases} (D/D_T)^{N_1} & D \leq 3.81 \text{ m} \\ (3.81/D_T)^{N_1}(D/3.81)^{N_1-\Delta} & D \geq 3.81 \text{ m} \end{cases}$$

$$C_{S2} = \left(\frac{1+(J_T/0.4)^2}{1+(J/0.4)^2}\right)\left(\frac{J_B\rho_B + J_P\rho_P}{J_P\rho_P}\right)\exp[-c_s(U_k - U_T)]$$

where c_s is the cushioning factor for self-breakage.

Experimental data

Ball × mill breakage

The material used for the simulations was a composite sample of copper ore from the Los Bronces mine in Chile. The standard method of determination of breakage parameters in a small laboratory mill as described by Austin, Klimpel and Luckie[1] was used, giving the characteristic parameters shown in Table 1.

Self-breakage parameters

The relations governing the variation of self-breakage parameters with mill conditions are not as well developed as those for ball milling, so a series of tests was performed using a readily

TABLE 1. Breakage parameters for copper ore determined in a laboratory mill

Conditions	Parameters
D = 194 mm	α = 0.95
d = 27 mm	Λ = 3.3
J_B = 0.20	μ = 1.65 mm
U = 0.5	$_T$ = 1.0 min^{-1}
Volume solid % = 40	γ = 0.70
Ore density = 2.77t/m^3	β = 4
Mill speed = 75% c.s.	Φ = 0.36

These values were also used to predict normal breakage by pebbles using the conversions of Eq. [13] and [14].

available and homogeneous material, a white crystalline quartz from the mine of the Castastone Company, North Carolina, with a Bond work index of 19 kWh/ton metric. These tests were with particular reference to elucidating the action of fracture breakage, chipping and abrasion during autogenous grinding. The test mill used was 0.6 m in diameter and 0.3 m long, fitted with 20 lifters. An adsorbable dye was used to number the feed material, and the weight of individual lumps followed as a function of grinding time in batch grinding tests. The weights were expressed as equivalent spherical radii to enable the calculation of abrasion rates.

Figure 5 shows typical results. To avoid the variation of parameters caused by the cushioning action of fine material and the decrease of mill charge, the tests were performed dry, the fine material was removed after short grinding periods, and the equivalent weight of unmarked fresh lumps added to preserve the desired J value. This type of test enables the linear decrease of weight due to abrasion to be readily determined, and values were averaged to obtain mean abrasion rates κ mm/min. Sudden changes in weight represented chipping of fragments from a lump, whereas complete disappearance from the size interval represented a disintegrative fracture.

The results indicated that pure abrasion gave relatively low rates of weight loss, so abrasion and chipping were combined to give an overall chipping-abrasion rate. Figure 6 illustrates the process in terms of the mass balances involved in the derivation of Eq. [8]. Figure 7 shows a typical result of the balance between average mass loss by fracture by fragments from chipping-abrasion and by cores wearing into the next smaller size internal. It is concluded that the proportion between these mechanisms remains constant during the process. Table 2 shows the variation of these ratios for a series of tests. The ratio of the mass lost as chipped fragments to that lost by cores for the $_4\sqrt{2}$ size intervals is expected to be about 33% since the distribution of mass is linear over the $_4\sqrt{2}$ interval.[7]

However, Figure 8 shows that the overall specific rate of breakage of traced lumps decreases with time even though the conditions in the mill are kept approximately constant. The equivalent decrease can also be seen in the pure abrasion rates in Figure 5. The physical process involved is quite clear. The raw feed lumps are irregular and some have a relatively high surface area per unit weight, thus they abrade and chip relatively rapidly. Chipping-abrasion causes the lumps to become rounded into pebbles, which chip-abrade more slowly. The direct proportionality of Figure 7 shows that the fracture component follows suit, so that the system behaves like a mixture of weaker material which disappears more rapidly, leaving stronger rounded

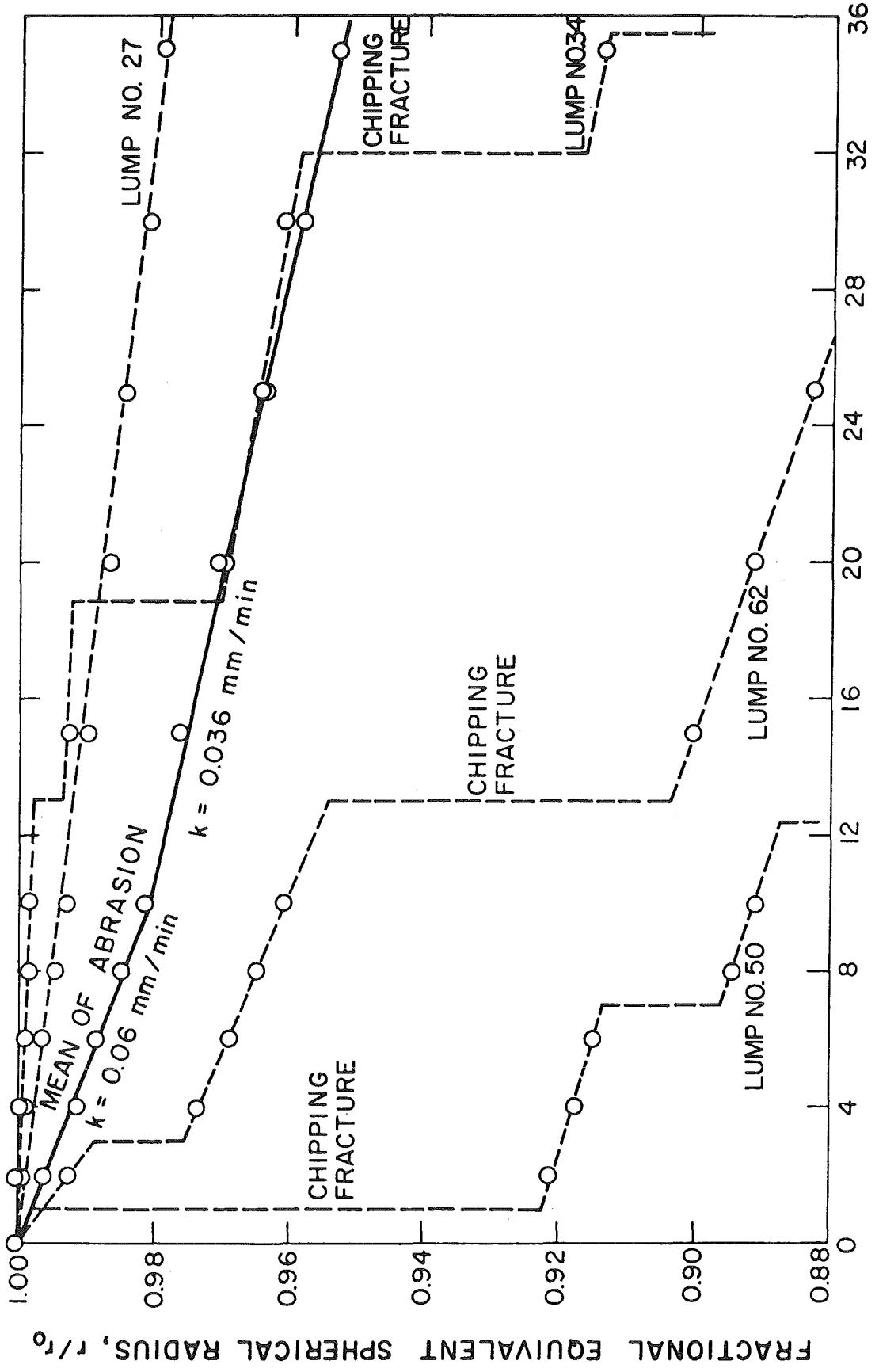

FIGURE 5. Change of equivalent spherical radius with time for 86 individually-traced lumps within the sieve range 63 × 53 mm; mean R_o = 31 mm, upper r_o = 35 mm, lower r_o = 27 mm (D = 0.6 m, fine material removed after grinding period)

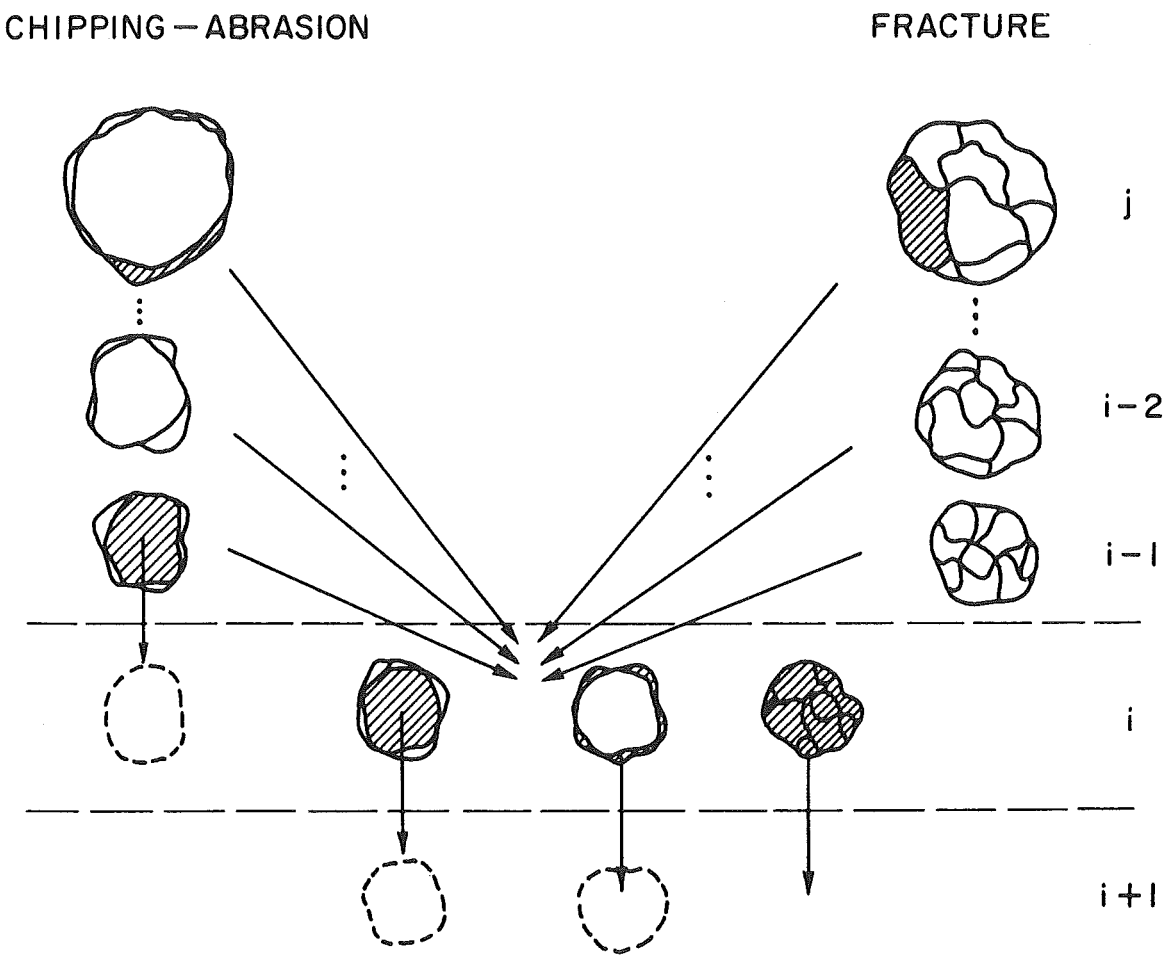

FIGURE 6. Illustration of mass balances of chipping-abrasion and fracture in autogenous breakage

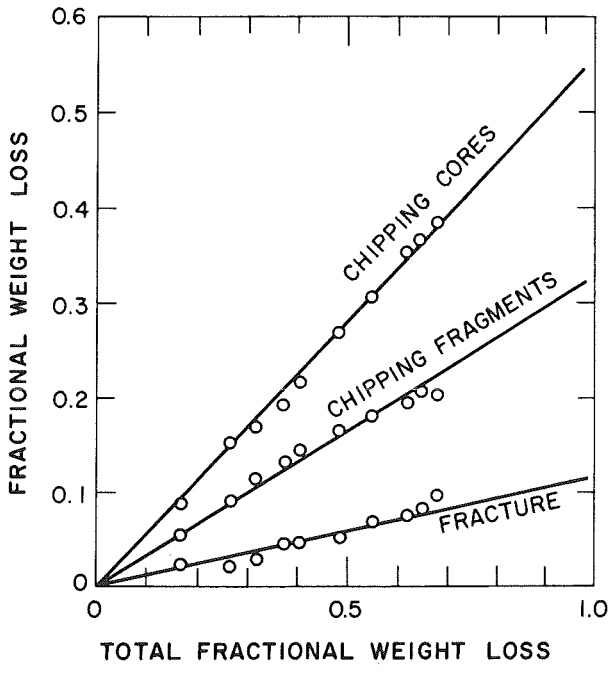

FIGURE 7. Contribution of individual breakage mechanisms to the total fractional weight loss. Fully autogenous test in a 0,6 m diameter mill. Quartz lumps of 63 × 53 mm in diameter, U = 0, J = 0.30, ϕ_c = 0.70

pebbles, which disappear more slowly.

Figure 8 also shows the strong influence of the accumulation of fine material, since the breakage rates with U=0.8 are far slower than for U=0.3. Figure 9 shows a typical result considered as a simple binary mixture: this is surely an approximation but it is sufficient for our present purpose. The squares are showing that the breakage rate of fresh rock is proportional to the fraction of fresh rock present, that is, its breakage follows a first-order law. Figure 10 shows breakage results in the presence of a varying quantity of balls to increase the mean density of the load. As expected, the net mill power is directly proportional to the mean density of the load, and the specific breakage rates are also proportional, validating Eq. [7].

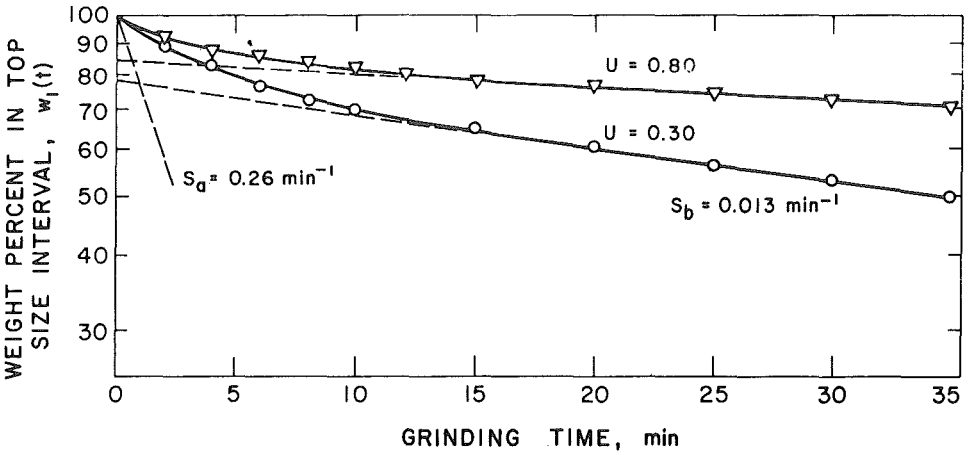

FIGURE 8. Rates of self-breakage for 26.5 × 22.4 mm copper ore. Dry batch autogenous grinding D = 0.6 m, ϕ_c = 0.7, J = 0.2, powder minus 100 mesh

TABLE 2. Deconvolution of chipping and fracture (quartz; D=0.6 m)

	Steel balls		Pebbles		Powder		Relative Breakage			
Test	Size mm	J_B	Size mm	J_P	Size mesh	U	Fracture	Cores	Chips	Chips/ (Cores+Chips)
1	-	-	65x53	0.30	-	-	0.14	0.56	0.30	0.35
2	-	-	53x45	0.30	-	-	0.12	0.57	0.31	0.35
3	-	-	45x38	0.30	-	-	0.13	0.57	0.30	0.34
	-	-	53x45	0.15	-	-	0.23	0.51	0.25	0.33
5-B	-	-	45x38	0.15	-	-	0.17	0.64	0.19	0.23
6-C	-	-	45x38	0.10	-	-	0.16	0.61	0.23	0.27
7	63x53	0.07	53x45	0.23	-	-	0.18	0.55	0.27	0.33
8	45x38	0.07	53x45	0.23	-	-	0.23	0.48	0.29	0.38
9	53x45	0.07	53x45	0.23	-	-	0.33	0.44	0.23	0.34
10	45x38	0.07	45x38	0.23	-	-	0.17	0.61	0.22	0.26
11	63x53	0.07	63x53	0.23	-	-	0.37	0.41	0.22	0.36
12	-	-	53x45	0.30	-100#	0.15	0.29	0.45	0.26	0.37
14	-	-	53x45	0.30	-100#	0.45	0.21	0.47	0.32	0.40
15	-	-	53x45	0.30	-100#	0.30	0.28	0.57	0.15	0.21
16	-	-	38x31	0.30	-	-	0.20	0.48	0.32	0.40
17	-	-	31x27	0.30	-	-	0.08	0.67	0.25	0.27
18	-	-	27x22	0.30	-	-	0.14	0.58	0.28	0.33
19-A	-	-	63x53	0.05	-	-	0.27	0.58	0.15	0.21
19-B	-	-	53x45	0.05	-	-	0.13	0.73	0.14	0.16
19-C	-	-	45x38	0.05	-	-	0.10	0.75	0.15	0.17
19-E	-	-	38x31	0.05	-	-	0.26	0.47	0.27	0.36
19-F	-	-	31x27	0.05	-	-	0.16	0.58	0.26	0.31
19-G	-	-	27x22	0.05	-	-	0.32	0.44	0.24	0.35

Test 19 is a mixture of 6 different sizes of J_P = 0.30 total.

Figure 11 shows that the primary breakage distributions are approximately normalized with respect to the breaking size, but are very different for the fresh feed and the rounded pebbles. In addition, the shapes of the distributions are quite different from those of normal fracture, which is to be expected since the component of fracture is relatively small (see Table 2). The shape clearly corresponds to a mixture of fracture plus the cores and fragments produced by chipping-abrasion. An estimate

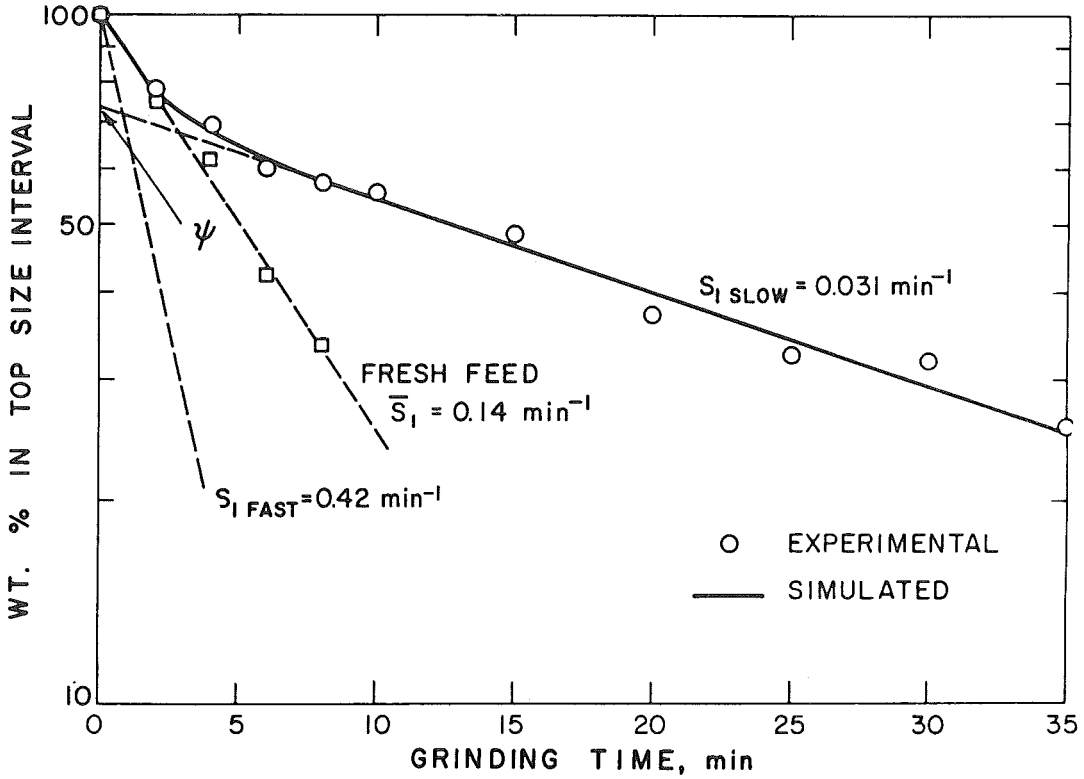

FIGURE 9. Determination of combined rate of breakage-chipping for 63 × 53 mm fresh feed (D = 0.6 m, J = 0.2, ϕ_c = 70% of critical speed, quartz, no accumulation of fines)

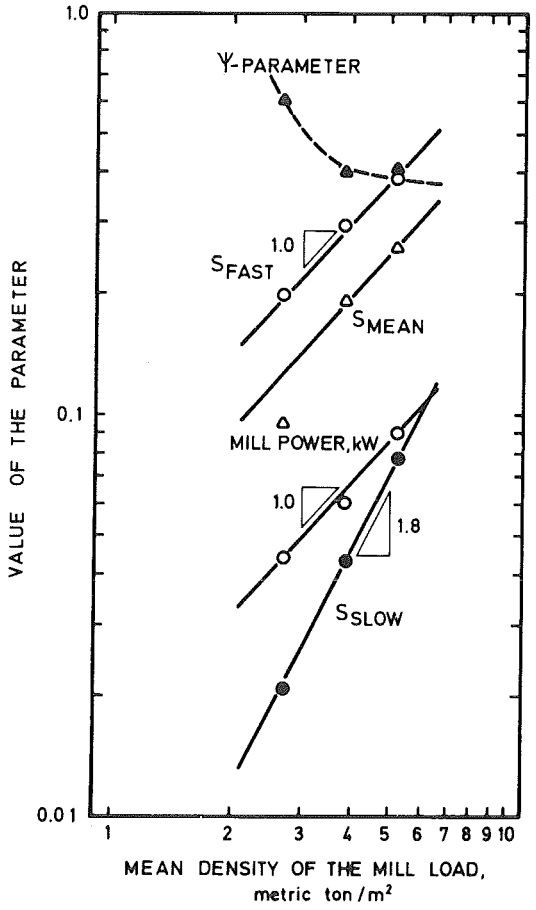

FIGURE 10. Variation of mill power and specific rates of self-breakage with density of the mill road: 53 × 45 mm quartz in 0.6 m diameter mill; 45 mm steel balls; J = 0.30

of the size distribution of abrasion-chipping fragments was made by rotating the mill at a low fraction of critical speed (45%) to give a flat angle and, hence, to reduce the impact forces of the tumbling. This gave the result shown in Figure 12 as self-abrasion.

It was also found that in a mixture of lump sizes, the presence of larger lumps increased the breakage rates of smaller lumps while the presence of smaller lumps decreased the breakage rates of larger lumps. No quantitative relation for this effect has yet been deduced.

The non first-order nature of the self-breakage as indicated in Figures 8 and 9 was found in all tests and complicates the analysis. The equivalent results for the copper ore were expressed as mean specific rates of breakage[14] defined by

$$S(S) = 1/(\frac{1-\psi}{S_A} + \frac{\psi}{S_B}) \qquad [19]$$

On this basis, the value of c_s was taken to be 1.3 and α_s=1. The value of $_{ST}$ was

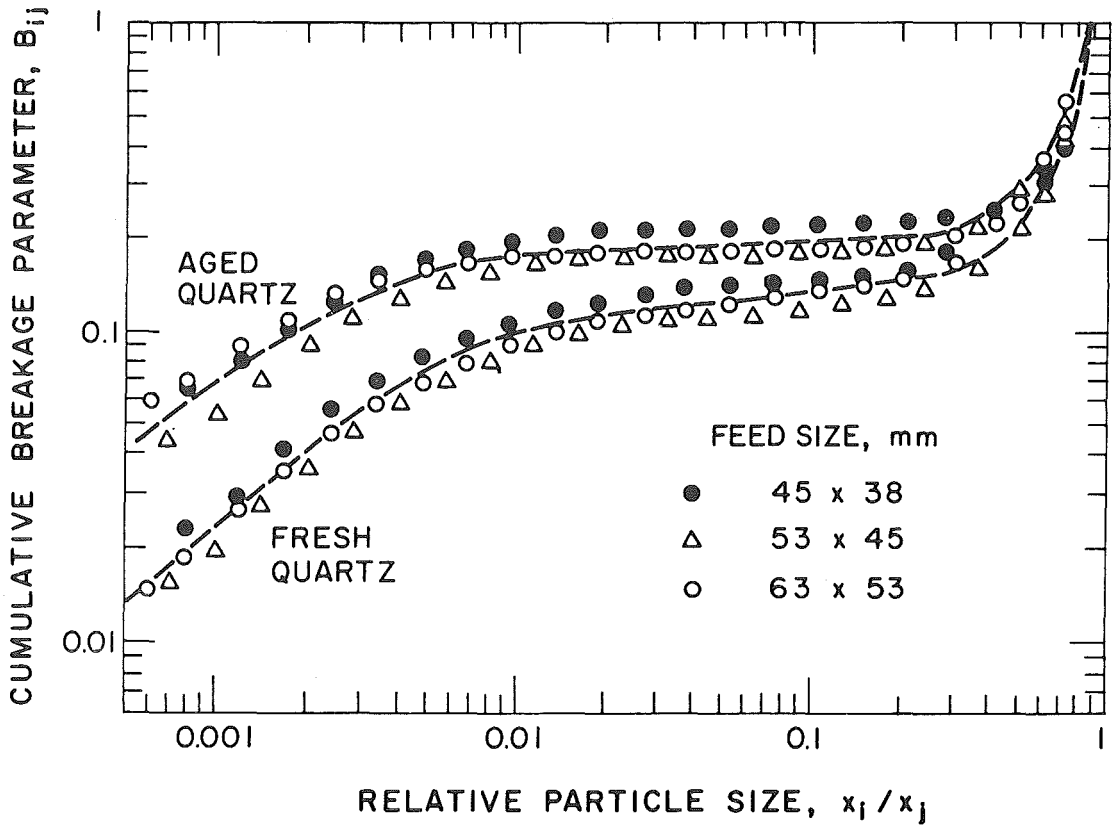

FIGURE 11. B values from fully-autogenous batch grinding tests in 0.6 m mills; J = 0.30, U = 0. ϕ_c = 0.7

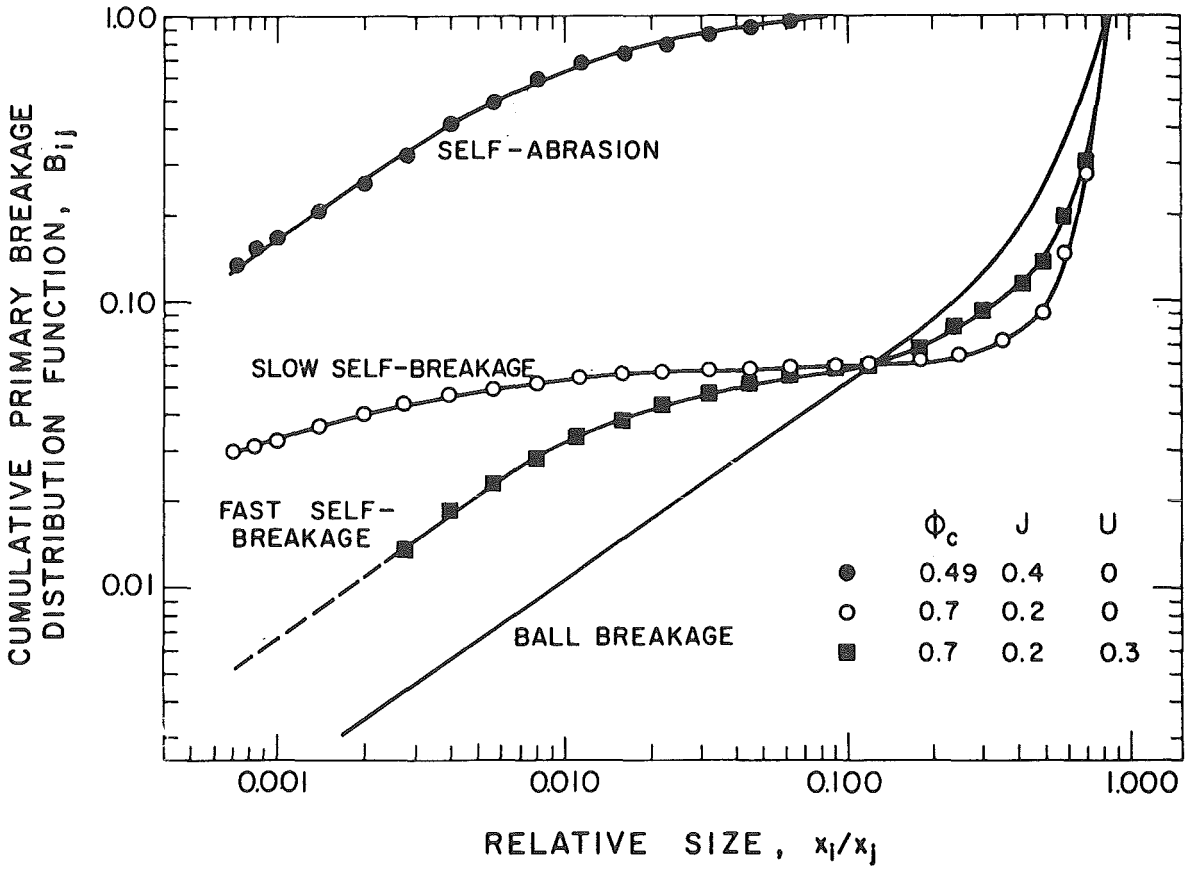

FIGURE 12. Cumulative primary breakage distribution values for 53 × 45 mm copper ore. Dry batch autogenous grinding in a 0,6 m diameter mill

determined by back-calculation[8] from steady-state continuous pilot-scale data to be 0.7 x 10^{-3} min^{-1} for a test mill diameter of 1.8 m and L/D=0.3, at J_T=0.2, ϕ_c=0.77 and approximately 40 volume % of solid in slurry leaving the mill.

Mass transport relations and grate classification

The continuous pilot-scale tests were also used to estimate the value of F_{vo} in Eq. [6]. This gave a value of $A_g k_m$ at f_{so}=0.25 of 0.37 $min^{-1} m^{0.5}$. On the other hand, the mass transport relation given for overflow ball mills[10] gives $k_m A_g$=0.5 h^{-1} $m^{0.5}$ for a solid filling level corresponding to approximately U=1 at J=0.38, which is about the same slurry filling. Thus, the SAG mill can pass large quantities of slurry without overfilling with slurry, by comparison with an overflow ball mill.

The comparison of size distributions within the pilot-scale to those leaving the mill gave a grate classification function of the form

$$c_i = 1/[1+(x_{50}/x_i)^{\lambda_g}] \quad [20]$$

For the 12 mm (half inch) grate opening, the values of the characteristic parameters were x_{50}=1.11 mm and λ_g=1.3. However, it must be understood that this action may be different in a full-scale mill where the grates are kept freely open by an adequate discharge mechanism. In this case, the

TABLE 3. Values used in simulations

			B values for various breaking sizes							
			Self-Breakage			By pebbles and balls				
Size Interval	Size μm	Feed % Minus size	1-3	4	5-26	1-3	4-11	Pebbles 12-26	Balls 12-26	Classifier selectivity s_i
1	215500	100.0								
2	152380	97.8								
3	107750	86.4	.45	.49	.54(5)	.46	.59	.46	.4	1.0
4	76190	71.1	.36	.29	.36	.23	.42	.31	.25	1.0
5	53875	62.2	.28	.24(5)	.32	.17	.35	.25	.16	1.0
6	83095	53.0	.25	.20	.27	.16	.30	.20	.12.	1.0
7	26940	43.8	.22	.18	.26	.13	.29	.16(5)	.092	1.0
8	19050	35.7	.20(5)	.16	.25	.11	.28	.14(5)	.076	1.0
9	13470	30.0	.19	.15	.24	.099	.26	.12(5)	.066	1.0
10	9525	26.2	.17	.14(5)	.23	.089	.25	.10(5)	.050	1.0
11	6735	22.5	.15	.13	.22	.081	.24	.88	.039	1.0
12	4760	19.0	.13	.12	.21	.074	.23	.074	.035	1.0
13	3370	17.4	.12	.11	.20	.069	.21	.056	.025	1.0
14	2380	15.4	.10(5)	.10	.18	.062	.19	.045	.020	1.0
15	1680	13.8	.094	.089	.17	.058	.17	.034		0.98
16	1190	12.2	.082	.079	.15	.052	.16			0.98
17	840	10.8	.074	.067	.13	.048	.14			0.94
18	595	9.6	.063	.059	.12	.042	.12			0.84
19	420	8.4	.057	.050	.099	.038	.11			0.71
20	300	7.3	.051	.044	.086	.034	.090			0.59
21	210	6.4	.046	.036	.077	.030	.075			0.49
22	150	5.8	.042	.032	.065	.025	.065			0.41
23	105	5.0	.038	.029		.022	.052			0.35
24	75	4.5	.036			.020				0.31
25	53	4.1	.030			.017				0.29
26	38	3.6	.025			.015				0.26

action of the grates can be considered as close to ideal classification, which can be closely approximated by x_{50}=grate size and λ_g=4.

Full scale simulation

SAG mill: L/D = 0.5

The mill simulated was a nominal 28 feet by 14 feet mill, giving D=8.2 m, L/D=0.5 and an effective volume of 230 m^3. The feed and overflow trunnion diameters represented a filling level of 29% to the level of overflow, and the design criteria was 25% that is, J=0.25, and 76% of critical speed. The cumulative primary breakage values estimated from laboratory batch tests are given in Table 3, and were entered as matrices into the program. The simulator was supplied with the feed size distribution also shown in Table 3, and simulations were performed for nominal fractional hold-up(J_T) in the mill covering the range 0.2 to 0.4, using a ball charge of 50% of 76 mm (3 inch) and 50% of 100 mm (4 inch) diameter balls. The mill was closed with the external classifier selectivity values given in Table 3.

The variation of mill capacity with hold-up and ball charge is shown in Table 4, and Figure 13. The charge load of 0.25 volume fraction was taken as optimum since it gave a region where the capacity is not sensitive to ball load in the region J_B=4% to 8%. The power equation used was that given by Austin[16]

$$m_p = K(D^{3.5})(L/D)(J)(1-1.03J)(\phi_c - \frac{0.1\phi_c}{2^{9-10\phi_c}})\rho_c \quad ,kW \qquad [21]$$

where ρ_c is the overall density of the charge, including balls and slurry. This was calculated using the bed porosity obtained from the use of the Weymont voidage factors, as described by Austin. The value of K was taken as 10.6 for dimensions in meters and ρ_c in metric tons/m^3, to produce the mill power quoted

TABLE 4. Results of SAG mill simulations

J_B	J	Circulation Ratio	Capactiy Q, tph	Hold-up W tons	Product size distribution % < 35 mesh	400 mesh	kWh/t
0	10.2	2.1	135	39	90.0	31.5	12.0
	15.0	2.3	195	56	91.0	32.1	10.9
	19.8	2.5	255	72	92.0	32.7	10.5
	25.0	2.7	305	88	92.8	33.3	10.3
	30.1	2.9	340	105	93.7	34.2	10.3
	35.4	3.2	365	121	94.5	35.2	10.4
4	14.7	2.3	220	39	91.8	32.5	11.8
	18.8	2.5	305	56	90.9	31.9	10.0
	22.6	2.7	370	72	90.2	31.5	9.1
	27.6	2.9	425	88	89.8	31.4	8.9
	32.8	3.1	455	105	89.1	31.1	9.1
	38.1	3.4	465	121	88.3	30.8	9.2
8	18.8	2.0	280	39	92.9	33.2	13.3
	23.0	2.3	365	56	91.4	32.1	10.9
	26.9	2.6	435	72	90.3	31.5	9.7
	31.2	2.8	490	88	89.7	31.3	9.1
	36.6	3.0	520	105	88.9	31.0	9.2
12	22.9	1.7	305	39	93.8	34.0	14.4
	27.0	2.1	415	56	92.1	32.5	11.7
	31.0	2.4	475	72	90.7	31.7	10.3
	35.0	2.7	525	88	89.8	31.4	9.6

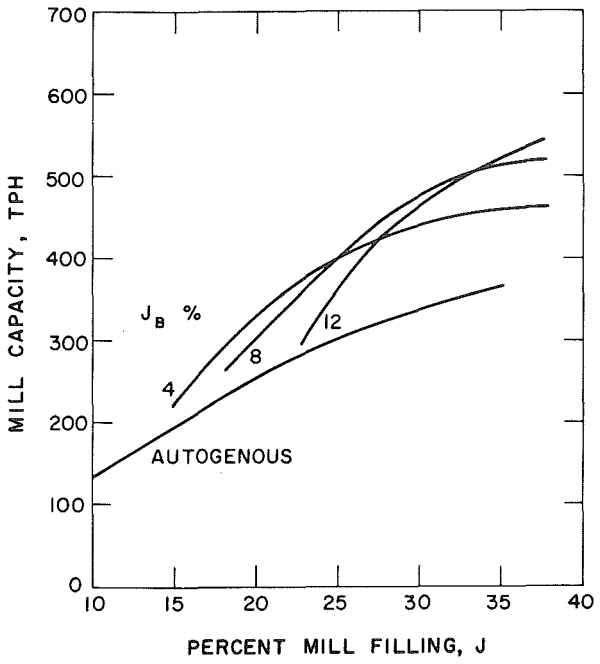

FIGURE 13: Variation of predicted mill capacity with filling and ball load for nominal 28 feet diameter by 14 feet long SAG mill

by Tanaka and Tanaka.[15]

The values of specific grinding energy in kWh/ton are also given in Table 4, and Figure 14 shows that the minimum occurs at about 6% ball load. Figure 15 shows the size distributions predicted by the model for operation at 8% ball load and for fully-autogenous operation. Figure 16 shows that the effect of the balls is to increase the specific rates of breakage of the larger sizes, while Figure 15 shows that the consequence is that the fraction

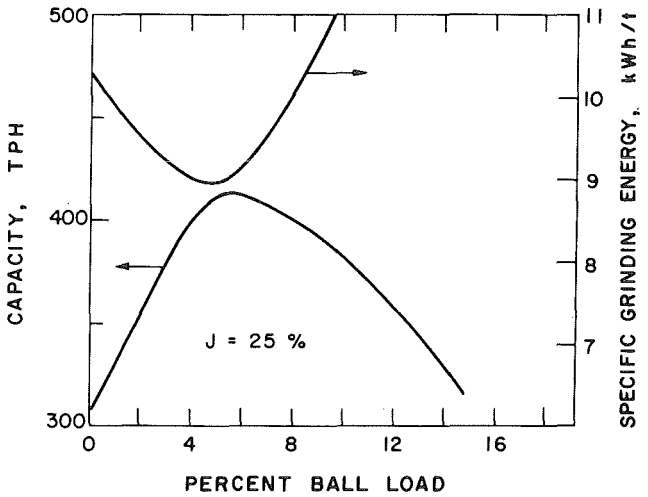

FIGURE 14. Optimum of capacity and specific grinding energy with ball load at total filling of 25% mill volume (see Fig. 13)

of mill charge in the size region of 20 mm to 60 mm is thus reduced.

FAG mill: L/D = 2.0

It was decided to compare the result with two equivalent FAG mills each pulling half of the SAG mill power, as predicted by the Bond equation for ball mills,

$$m_p = 7.33D^{3.3}(L/D)(J)(1-0.937J)\left(\phi_c \frac{0.1\phi_c}{2^{9-10\phi_c}}\right)\rho_b \text{ , kW} \quad [22]$$

where ρ_b is normally the ball density but in this case was the ore density of 2.77 tons/m^3. L/D was assumed to be 2.0, ϕ_c=0.85, and the value of J was taken as 0.3. With these assumptions, the mill diameter is D = 5.6 m to give a mill shaft power of 2000 kW.

The simulation was performed with the same breakage parameters used for the SAG milling, the same grate openings to retain large material and the same external classifier function. The feed to the 5.6 m internal diameter FAG mill was taken as the same as that to the SAG mill.

No information was available for the expected mass transport relation, but the comparison of the values for the SAG mill with those for overflow mills suggests that the long L/D mills fill up with slurry to a greater extent than the SAG mill, presumably due to the resistance to mass flow through the long length of tumbling charge. Thus, the value of f_{so} in Eq. [4] was increased arbitrarily by a factor of 3. Table 5 gives the results. The specific grinding energy is substantially less, but this result is sensitive to the mass transport factor so it is not possible to assert this with a high degree of confidence. In addition, it may not be valid to use the Bond power equation for a pebble mill, since it predicts a much lower mill power than equation 21.

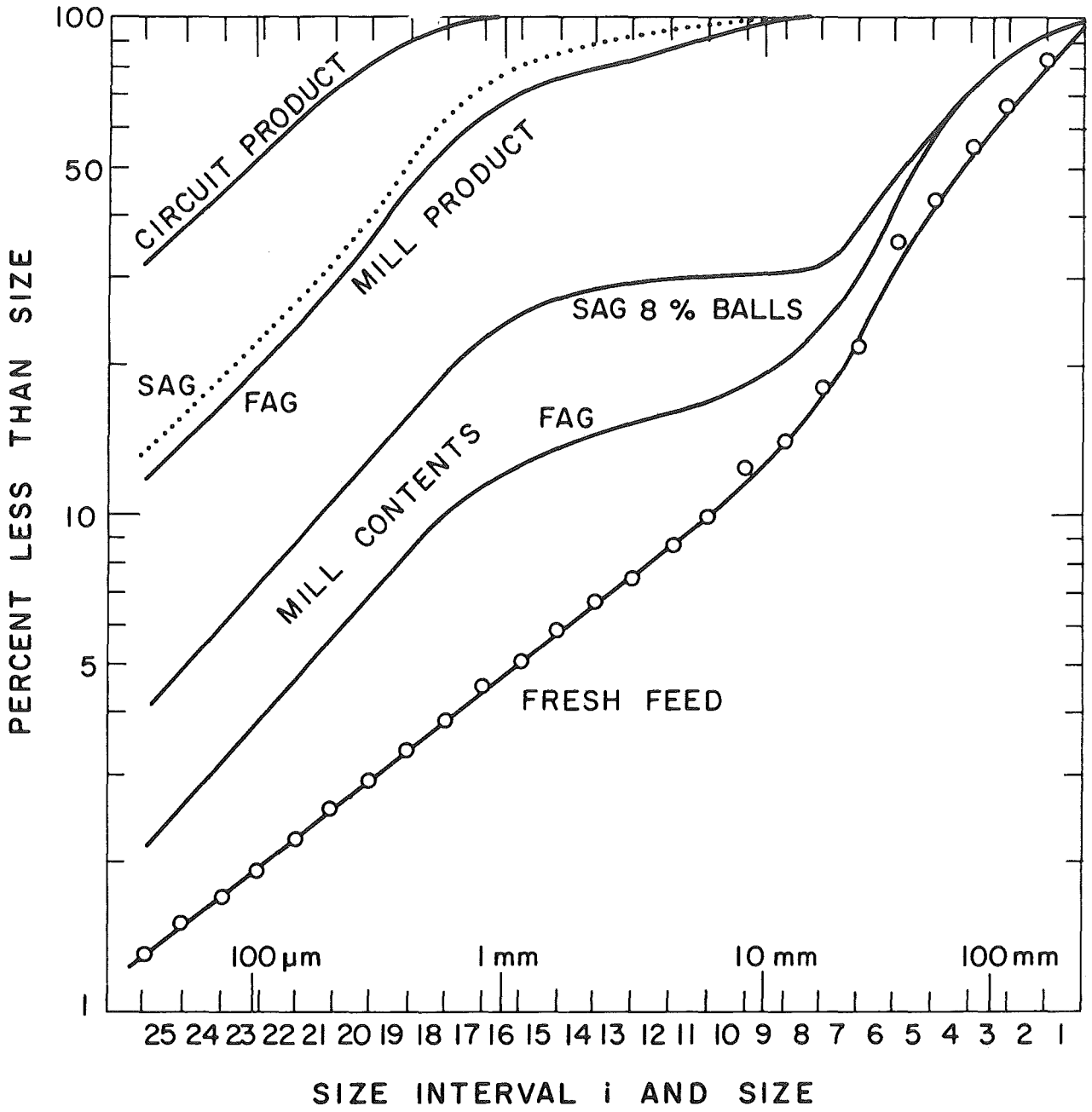

FIGURE 15. Simulated size distributions for SAG mill (see Fig. 13) with 8% ball load and 0% ball load

TABLE 5. Results of simulations of 5.6 m diameter FAG mill (L/D = 2.0)

Nominal fractional hold-up	0.3
% minus 35 mesh in circuit	89
% minus 400 mesh in circuit product	31
Output Q, tph	270
Circulation ratio C	3.7
Mill hold-up,t	140
Mill power, kW	2000
Specific grinding energy, kWh/t	7.4

Discussion of results

It is clear that the ore studied was a coherent ore which would be suitable for FAG grinding since it leads to a mill charge with sufficient large rounded pebbles to be equivalent to a ball mill (with lower density of media, of course). Although the specific rates of breakage of these large lumps are relatively low, requiring larger mill volume as compared to ball milling, the chipping-abrasion process

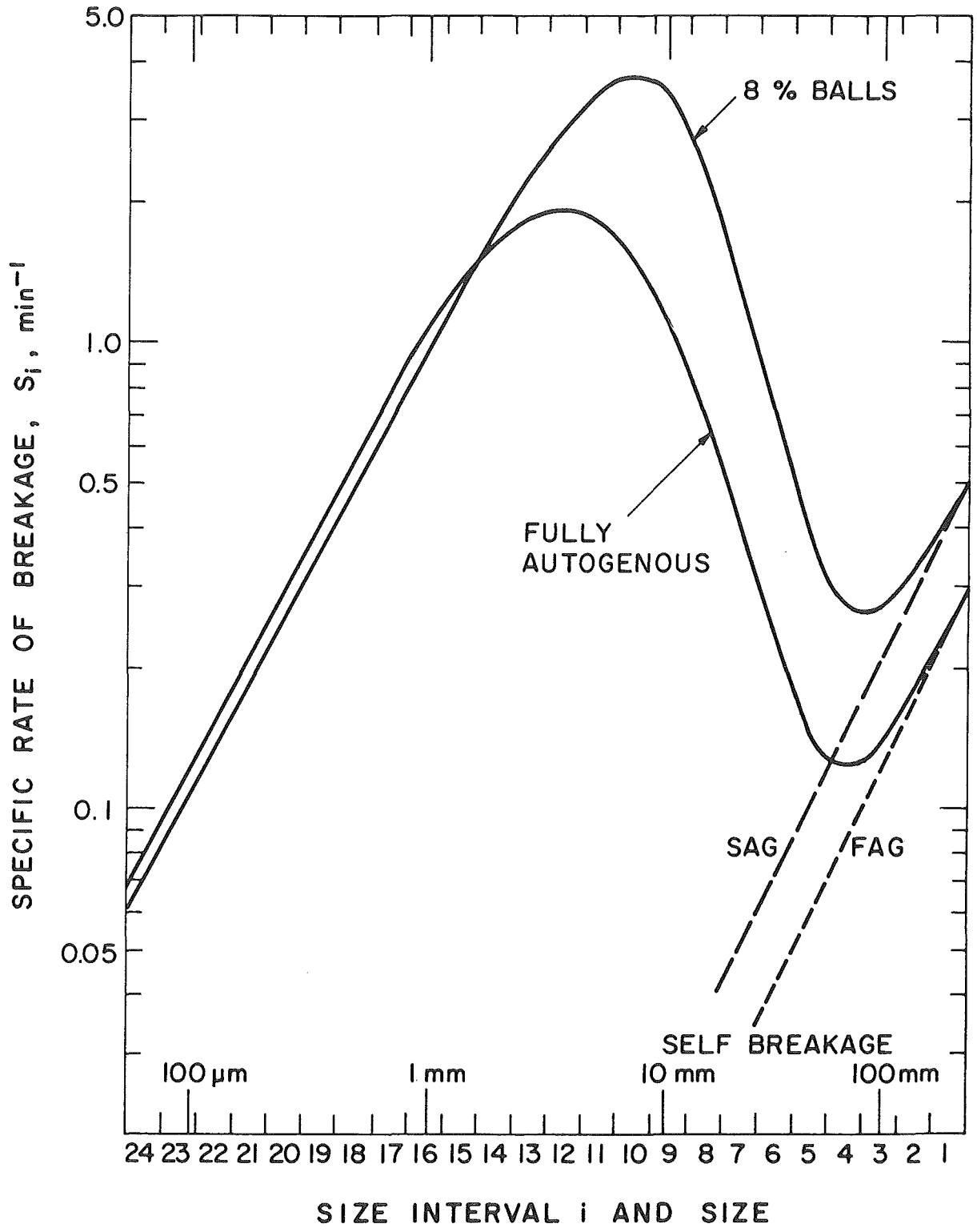

FIGURE 16. Simulated specific rates of breakage for conditions of Figure 15

produces a high proportion of fines which compensates for the low breakage rates to give specific grinding energies and circuit products comparable to more conventional crushing-grinding circuits. However, the use of 6 volume % of ball charge and a total fractional mill charge of 25 volume % gives a substantial increase in capacity (from 305 tph to 400 tph) over FAG milling in the large mill, with a significantly finer circuit product (approximately 32% minus 400 mesh versus 33%) and somewhat

lower circulating load.

The long L/D FAG mills gave similar circuit product size distributions, but required two mills of 5.6 m diameter to perform the same duty as the one 8.2 m diameter SAG mill. Clearly, for this type of ore, the choice of system depends on the comparative economic calculations of capital and interest cost and steel consumption.

There remains substantial work to be done to improve the model to a level of accuracy sufficient for utility. The use of average specific rates of self-breakage is not as satisfactory as the use of equations representing a fast-slow breakage process. The current method of entry of B values is not satisfactory. The lack of precise relations to describe the variation of S and B values with mill conditions prevents the development of simple laboratory tests to predict the values from a small amount of laboratory work. The results are sensitive to the level of slurry in the mill, but the calculation of this level by mass transport relations is based on entirely inadequate information. The model at the moment does not include the effect of ball diameter on self-breakage.

It will be interesting to program the model for removal of material from the mill contents by pebble ports, followed by crushing of these sizes, in the size range of 38 mm (1.5 inches) to 75 mm (3 inches). At the moment, it is not possible to demonstrate the effect of using a less coherent ore because the associated variation of the self-breakage B values is not known: the rapid breakage of a weak ore is expected to give B values with a smaller fraction of fines.

Acknowledgements

The work was performed under NSF Grant CPE 8303154.

References

1. AUSTIN, L.G., KLIMPEL, R.R. and LUCKIE, P.T. Process Engineering of Size Reduction: Ball Milling. New York, N.Y., Society of Mining Engineers of A.I.M.E., 1984, pp. 1-561.
2. STANLEY, G.G. Mechanisms in the autogenous mill and their mathematical representation. J. So. Afr. Inst. Min. Metal., Vol. 75, 4, Nov. 1974, pp. 77-98.
3. GAULT, G.A. Modelling and control of autogenous grinding circuits. Ph.D. Thesis, University of Queensland, Australia, 1974.
4. VANDERBEEK, J.L., HERBST, J.A., RAJAMANI, K. and HALES, L. Online estimation of particle size distribution and volumetric filling in a SAG mill with a view to automatic control. Presentation, Society of Mining Engineers of A.I.M.E. meeting in Alburquerque, N.M., Oct. 1985.
5. AUSTIN, L.G., WEYMONT, N.P., PRISBEY, K.A. and HOOVER, M. Preliminary results on the modeling of autogenous grinding. Proc. 14th Int. APCOM Conference. Ramani, R.V., The Pennsylvania State University, P.A., 1976, pp. 207-226.
6. AUSTIN, L.G., WEYMONT, N.P., BARAHONA, C.A. and SURAYANARAYAN, K. An improved simulation model for semi-autogenous grinding. Powder Technology, Vol. 47, 3, 1986, pp. 265-283.
7. AUSTIN, L.G., BARAHONA, C.A. and MENACHO, J.M. Fast and slow chipping fracture and abrasion in autogenous grinding. Powder Technology, Vol. 46, 1, 1986, pp. 81-87.
8. AUSTIN, L.G., BARAHONA, C.A. and MENACHO, J.M. Investigations of autogenous and semi-autogenous grinding in tumbling mills. Proc. 1st. World

Congress Particle Technology. Leschonski, K., Nuremberg, Federal Republic of Germany, April 1986.

9. HOYER, D.I. and AUSTIN, L.G. A simulation model for autogenous pebble mills, Society of Mining Engineers of A.I.M.E. meeting in Alburquerque, N.M., Oct. 1985.
10. ROGERS, R.S.C. and AUSTIN, L.G. Residence time distributions in ball mills. Particulate Science and Technology, Vol. 2,2, 1984. pp. 193-204.
11. AUSTIN, L.G. and CONCHA, F.A. Diseño simulación de circuitos de molienda. To be published.
12. MENACHO, J.M. Some solutions for the kinetics of combined fracture and abrasion breakage, Powder Technology, Vol. 49,1, 1986, pp. 87-95.
13. WEYMONT, N.P. The analysis and simulation of autogenous grinding systems, Ph.D. Thesis, The Pennsylvania State University, P.A., 1979.
14. AUSTIN, L.G., TRIMARCHI, T.J. and WEYMONT, N.P. An Analysis of some cases of non-first order breakage rates. Powder Technology, Vol. 17,1, 1977, pp. 109-113.
15. TANAKA, T. and TANAKA, K. Design features of a semi-autogenous grinding mill and a comparison of test mill data with actual operation data. Santiago, Chile, Centro de Investigación Mineva y Metalurgica, Primer Taller Nacional de Molienda Autogena de Minerales. Preprint No. 6, Sept. 1983, pp. 1-26.
16. AUSTIN, L.G. Chapter 14, Semi-autogenous (SAG) and fully autogenous grinding. Short course notes: Process Engineering of Size Reduction in Tumbling Mills, The Pennsylvania State University, P.A., September 1987, pp. 14.1-14.55.